

Learning Generalizable Hand-Object Tracking from Synthetic Demonstrations

YINHUI WANG*, HKUST, China
 RUNYI YU*, HKUST, China
 HOK WAI TSUI*, HKUST, China
 XIAOYI LIN*, Wuhan University, China
 HUI ZHANG, ETH Zurich, Switzerland
 QIHAN ZHAO, HKUST, China
 KE FAN, Shanghai Jiao Tong University, China
 MIAO LI, Wuhan University, China
 JIE SONG, HKUST (Guangzhou), China
 JINGBO WANG, Shanghai AI Lab, China
 QIFENG CHEN[†], HKUST, China
 PING TAN[†], HKUST, China

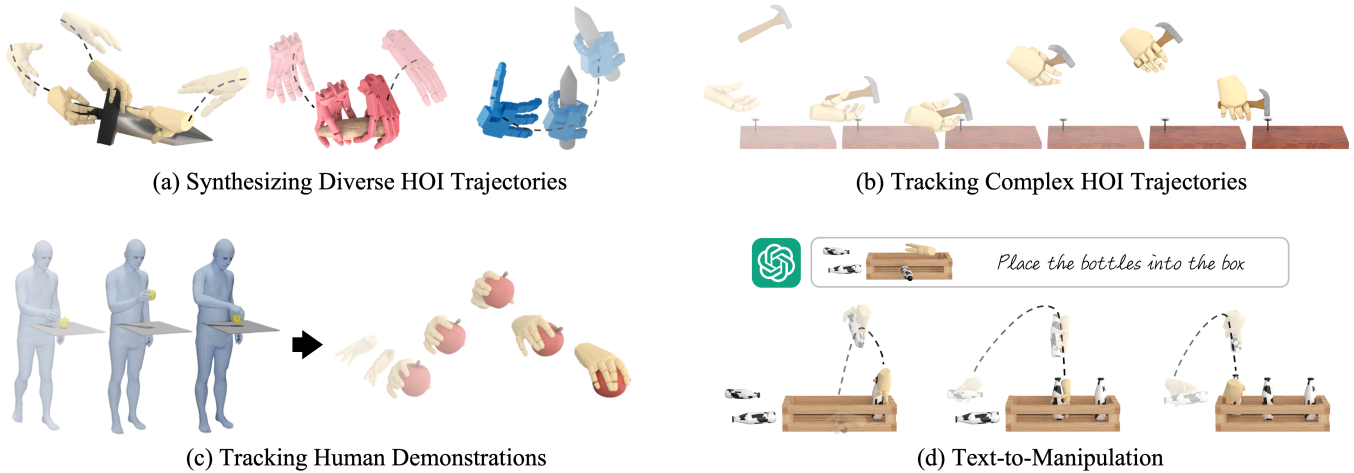


Fig. 1. Our system synthesizes and tracks hand-object trajectories for a variety of dexterous skills—such as grasping, placing, and in-hand reorientation—as well as their combinations. The approach generalizes across diverse hand and object morphologies and, notably, transfers flexibly to downstream applications including human motion tracking and text-guided task execution. We encourage readers to view our project page: <https://ingrid789.github.io/hot/>

Authors' Contact Information: Yinhuai Wang*, HKUST, Hong Kong, China, yinhuai.wang@connect.ust.hk; Runyi Yu*, HKUST, Shanghai, China; Hok Wai Tsui*, HKUST, Hong Kong, China; Xiaoyi Lin*, Wuhan University, Wuhan, China; Hui Zhang, ETH Zurich, Zurich, Switzerland; Qihan Zhao, HKUST, Hong Kong, China; Ke Fan, Shanghai Jiao Tong University, Shanghai, China; Miao Li, Wuhan University, Wuhan, China; Jie Song, HKUST (Guangzhou), Guangzhou, China; Jingbo Wang, Shanghai AI Lab, Shanghai, China; Qifeng Chen[†], HKUST, Hong Kong, China, cqf@ust.hk; Ping Tan[†], HKUST, Hong Kong, China, pingtan@ust.hk.

Permission to make digital or hard copies of all or part of this work for personal or classroom use is granted without fee provided that copies are not made or distributed for profit or commercial advantage and that copies bear this notice and the full citation on the first page. Copyrights for components of this work owned by others than the author(s) must be honored. Abstracting with credit is permitted. To copy otherwise, or republish, to post on servers or to redistribute to lists, requires prior specific permission and/or a fee. Request permissions from permissions@acm.org.

© 2025 Copyright held by the owner/author(s). Publication rights licensed to ACM.
 ACM XXXX-XXXX/2025/12-ART
<https://doi.org/10.1145/nnnnnnn.nnnnnnn>

We present a system for learning generalizable hand-object tracking controllers purely from synthetic data, without requiring any human demonstrations. Our approach makes two key contributions: (1) HOP, a Hand-Object Planner, which can synthesize diverse hand-object trajectories; and (2) HOT, a Hand-Object Tracker that bridges synthetic-to-physical transfer through reinforcement learning and interaction imitation learning, delivering a generalizable controller conditioned on target hand-object states. Our method extends to diverse object shapes and hand morphologies. Through extensive evaluations, we show that our approach enables dexterous hands to track challenging, long-horizon sequences including object re-arrangement and agile in-hand reorientation. These results represent a significant step toward scalable foundation controllers for manipulation that can learn entirely from synthetic data, breaking the data bottleneck that has long constrained progress in dexterous manipulation.

CCS Concepts: • **Computing methodologies** → **Procedural animation; Control methods; Robotics.**

Additional Key Words and Phrases: reinforcement learning, dexterous hands, dexterous manipulation, hand-object interaction

ACM Reference Format:

Yinhuai Wang*, Runyi Yu*, Hok Wai Tsui*, Xiaoyi Lin*, Hui Zhang, Qihan Zhao, Ke Fan, Miao Li, Jie Song, Jingbo Wang, Qifeng Chen[†], and Ping Tan[†]. 2025. Learning Generalizable Hand-Object Tracking from Synthetic Demonstrations. 1, 1 (December 2025), 17 pages. <https://doi.org/10.1145/nnnnnnn.nnnnnnn>

1 Introduction

The ability to track and execute complex, dynamic hand-object interaction (HOI) with human-like dexterity is crucial for robots to perform varied dexterous manipulation tasks. Traditional teleoperation systems typically track only the robot or hand motion without considering object states, resulting in poor performance for high-dynamic, precision-demanding tasks [Cheng et al. 2024; Fu et al. 2024]. By incorporating object states into the tracking control loop, hand-object state tracking [Liu et al. 2025; Wang et al. 2023a, 2025; Xu et al. 2025; Yin et al. 2025] significantly enhances the agility and robustness of task execution. However, training a generalizable hand-object tracking controller faces the fundamental challenge of acquiring sufficient HOI data. Such data typically relies on human demonstrations, which are either labor-intensive to collect through motion capture devices [Fan et al. 2023; Kim et al. 2024] or difficult to control for quality and distribution when estimated from internet videos [Cao et al. 2021; Wen et al. 2023].

In this paper, we address this data challenge by exploring novel ways to leverage synthetic data for training generalizable hand-object trackers. Our approach is built on three key insights: (1) Dexterous manipulation involves continuous transitions between hand-object states, particularly between different grasp configurations. While capturing such continuous interactions is difficult, static states like grasp configurations can be synthesized in large quantities [Liu et al. 2021; Wang et al. 2023b; Zhang et al. 2024a]. We capitalize on this asymmetry by generating synthetic manipulation sequences through the transformation, interpolation, and concatenation of these static key frames into plausible pseudo-demonstrations. (2) Although synthetic data may contain physical implausibilities, recent advances in combining reinforcement learning and imitation learning have demonstrated a notable robustness to imperfect demonstrations [Wang et al. 2023a, 2025; Xu et al. 2025; Yu et al. 2025]. This finding provides strong support for the effective utilization of imperfect synthetic data. (3) Tracking systems can be trained effectively on disconnected sequences of meta-skills, rather than on long, semantically complete tasks. For instance, instead of modeling “grasping a hammer and hammering a nail,” we synthesize elemental skills like Grasp, Rotate, and Move. This decomposition bypasses the need for complex task-level synthesis and results in a tracker that generalizes to diverse long-horizon tasks at inference time.

Based on these insights, we present HOP (Hand-Object Planner), a scalable manipulation data synthesis framework for generating diverse hand-object trajectories across various object shapes and hand morphologies, and HOT (Hand-Object Tracker), a tracking-based controller trained on these demonstrations, capable of tracking complex, highly dynamic, and long-sequence manipulation trajectories during inference. HOP generates synthetic meta-skill trajectories

through a structured, two-stage process. First, given a rigid object and a dexterous hand model, it employs force-closure optimization and reinforcement learning [Wang et al. 2023b; Zhang et al. 2024a] to generate and refine a diverse set of stable grasp configurations. Subsequently, HOP anchors itself to these grasp poses to synthesize trajectories for fundamental meta-skills—such as Grasping, Moving, Placing, and Rotating—as well as their combinations. HOT is trained primarily on the meta-skill data synthesized by HOP, using a unified set of HOI imitation rewards. To enhance model capacity and learning efficiency, we introduce a two-stage teacher-student training framework, coupled with a data randomization curriculum that progressively increases the randomness of training samples—such as varying object sizes and initial poses—as the model converges, thereby improving overall robustness.

Our experimental results demonstrate that HOT, trained exclusively on synthetic data from HOP, exhibits remarkable generalization across the entire operational space. It robustly tracks long-horizon, dynamic sequences—such as catching a thrown hammer, reorienting it in-air, and performing a hammering motion. Moreover, HOT shows effectiveness in tracking real human demonstrations [Taheri et al. 2020] and data from HOI generative models [Cha et al. 2024]. Notably, the system enables zero-shot transfer to downstream applications. When integrated with LLMs or VLMs [Achiam et al. 2023; Team et al. 2023], it follows language instructions to control both HOP-based data synthesis and HOT’s tracking for goal-directed manipulation. Overall, this work constitutes a significant advance toward general-purpose foundation controllers for dexterous manipulation.

2 Related Work

Reinforcement Learning for Dexterous Manipulation. Recent years have witnessed significant progress in dexterous manipulation, particularly in grasping tasks [Allshire et al. 2022; Andrychowicz et al. 2020; Chen et al. 2023a,b; Fang et al. 2023; Huang et al. 2023; Rajeswaran et al. 2018; She et al. 2022, 2024; Yin et al. 2023]. By leveraging advances in reinforcement learning [Schulman et al. 2017] and simulation technology [Makoviychuk et al. 2021; Todorov et al. 2012], current grasp models can handle objects of varying shapes [Wan et al. 2023; Xu et al. 2023; Zhang et al. 2024a]. However, these approaches typically rely on task-specific reward engineering, limiting their generalization to broader manipulation tasks [Chen et al. 2023b]. While similar paradigm have shown impressive results in specific dexterous tasks like object reorientation [Andrychowicz et al. 2020] and articulated object manipulation [Zhang et al. 2024b], they struggle to scale to general manipulation scenarios. Some methods attempt to enhance task diversity through mixture of experts, but they still cannot circumvent the labor-intensive nature of task-specific reward engineering [Yang et al. 2020]. Recently, [Chen et al. 2024; Liu et al. 2025; Wang et al. 2023a, 2025; Xu et al. 2025] propose a paradigm shift by introducing general imitation rewards to mimic robot-object state trajectories, enabling unified learning across different manipulation tasks. Notably, this paradigm demonstrates impressive robustness to data imperfections and high data efficiency, substantially reducing requirements for demonstration

quality and quantity. However, acquiring diverse manipulation data remains a significant challenge.

Demonstration Data for Dexterous Manipulations. Data collection remains a critical challenge for learning dexterous manipulation skills. Current approaches primarily fall into two categories: human demonstrations and synthetic data generation.

Human demonstrations are typically collected through teleoperation, device-based motion capture, and video-based estimation. While teleoperation provides accurate action data, it suffers from latency and perception barriers, making agile and precise manipulations challenging [Cheng et al. 2024; Fu et al. 2024; He et al. 2024]. Motion capture system using specialized sensor gloves and camera arrays can capture detailed hand-object motion [Banerjee et al. 2024; Fan et al. 2023; Taheri et al. 2020], but incurs significant time and labor costs. Recent advances in video-based pose estimation enable extraction of hand-object motion from vast video datasets [Cao et al. 2021; Wang et al. 2023a; Wen et al. 2023], however these methods often struggle with occlusion and depth ambiguity.

Synthetic data generation has gained increasing attention recently [Gao et al. 2024; Garrett et al. 2024; Jiang et al. 2024; Mandlekar et al. 2023; Pumacay et al. 2024], with methods mainly focusing on transforming and recombining existing reference data [Garrett et al. 2024; Jiang et al. 2024; Mandlekar et al. 2023]. While these approaches increase combination diversity, they fundamentally cannot generate novel manipulation patterns and still require human demonstrations as reference. In contrast, we propose a procedural generation approach that synthesizes basic manipulation patterns from static grasps, which are widely available. Through the synergy of reinforcement learning and imitation learning, our method effectively refines these synthetic trajectories to ensure physical plausibility. While human demonstrations can provide valuable reference when available, our approach demonstrates that a generalizable hand-object tracking policy can be learned without relying on such data, offering superior scalability and flexibility in scenarios where human demonstrations are scarce or impractical to collect.

3 Method

We propose a system for generalizable hand-object tracking purely from synthetic demonstrations. Our system consists of two parts: HOP (Hand-Object Planner), a scalable data generation framework, and HOT (Hand-Object Tracker), a tracking-based controller trained on synthetic data, capable of tracking complex, highly dynamic, and long-sequence manipulation trajectories during inference. In applications, our system achieves flexible tasks through a modular pipeline. First, a high-level directive—such as a text command processed by an VLM, a trajectory from a HOI generative model, or a captured human demonstration—is converted into a set of sparse waypoints. These waypoints are then fed to our planner, HOP, which generates a dense hand-object trajectory. Finally, our tracking controller, HOT, executes this trajectory in the simulation. This standardized workflow allows for zero-shot adaptation to numerous downstream applications. Fig. 2 presents an overview of our system architecture.

3.1 Hand-Object Planner

The Hand-Object Planner (HOP) consists of two steps: first, synthesizing stable grasp configurations, and second, generating meta-skill demonstrations or their combinations based on these grasp configurations. Fig. 3 illustrates our data generation pipeline. We now detail each component.

3.1.1 Synthesizing Grasp Pose Candidates. Static grasp configurations can be easily obtained from existing dataset [Chao et al. 2021; Fan et al. 2023; Hasson et al. 2019; Taheri et al. 2020; Wang et al. 2023b], grasp models [Miller and Allen 2004; Wan et al. 2023; Xu et al. 2023; Zhang et al. 2024a], or through optimization [Liu et al. 2021; Wang et al. 2023b], thereby ensuring substantial scalability potential. In this study, we leverage a off-the-shelf grasp generator [Wang et al. 2023b] driven by differentiable force closure estimation [Liu et al. 2021] to generate diverse grasp configurations. Specifically, given a rigid object and a dexterous hand, we obtain a set of grasp configurations $\hat{\mathcal{G}} = \{\mathbf{g}_1, \mathbf{g}_2, \dots, \mathbf{g}_M\}$. The grasp configuration is parameterized by hand-object state

$$\mathbf{g} = \{\mathbf{T}^h, \mathbf{R}^h, \boldsymbol{\theta}, \mathbf{P}^h, \mathbf{T}^o, \mathbf{R}^o, \mathbf{P}^o\}. \quad (1)$$

Taking the MANO hand model [Romero et al. 2017] as an example, $\mathbf{T}^h \in \mathbb{R}^3$ and $\mathbf{R}^h \in SO(3)$ represent the global wrist pose, while $\boldsymbol{\theta} \in \mathbb{R}^{15 \times 3}$ describes the joint angles of the five fingers (each finger has three joints with three degrees of freedom). $\mathbf{P}^h \in \mathbb{R}^{15 \times 3}$ denotes the global positions of finger joints. Similarly, \mathbf{T}^o , \mathbf{R}^o , and $\mathbf{P}^o \in \mathbb{R}^{N \times 3}$ represent the object’s global pose and the global positions of N keypoints on the object surface.

3.1.2 Filtering and Refining Grasp Poses. After obtaining a large set of initial grasp pose candidates, we train a coach policy to filter and refine them into physically plausible and stable configurations for subsequent data synthesis. Specifically, the policy is trained in simulation by initializing the hand and object according to each candidate pose. The coach policy is optimized using a grasp reward that encourages successful grasping and adherence to the original candidate pose. To enhance robustness, we apply random force perturbations to the object during training. Additional implementation details of the coach policy follow the setup described in Sec. 3.2. Once the policy converges, we collect the successful grasp poses generated during its rollouts as the stable grasp pose set \mathcal{G} . These refined poses are significantly higher in quality, physical realism, and stability compared to the original candidates.

3.1.3 Synthesizing Meta-Skill Trajectories. A dexterous manipulation trajectory is represented as $\boldsymbol{\tau} = \{\mathbf{g}_t\}_{t=0}^T$, with each \mathbf{g}_t parameterized as in Eq. 1. We synthesize pseudo-demonstrations by interpolating randomly generated hand-object states and grasp configurations. While these trajectories may be physically approximate, they serve as tracking targets in reinforcement imitation learning, enabling the policy to learn generalizable target-action mappings. For efficient synthesizing and learning, we decompose manipulation into eight meta-skills: Free Move, Grasp, Place, Move, Catch, Throw, Rotate, and Regrasp. Below, we detail the synthesis of Free Move, Grasp, Move, Place, and Rotate; see the Appendix for Catch, Throw, and Regrasp.

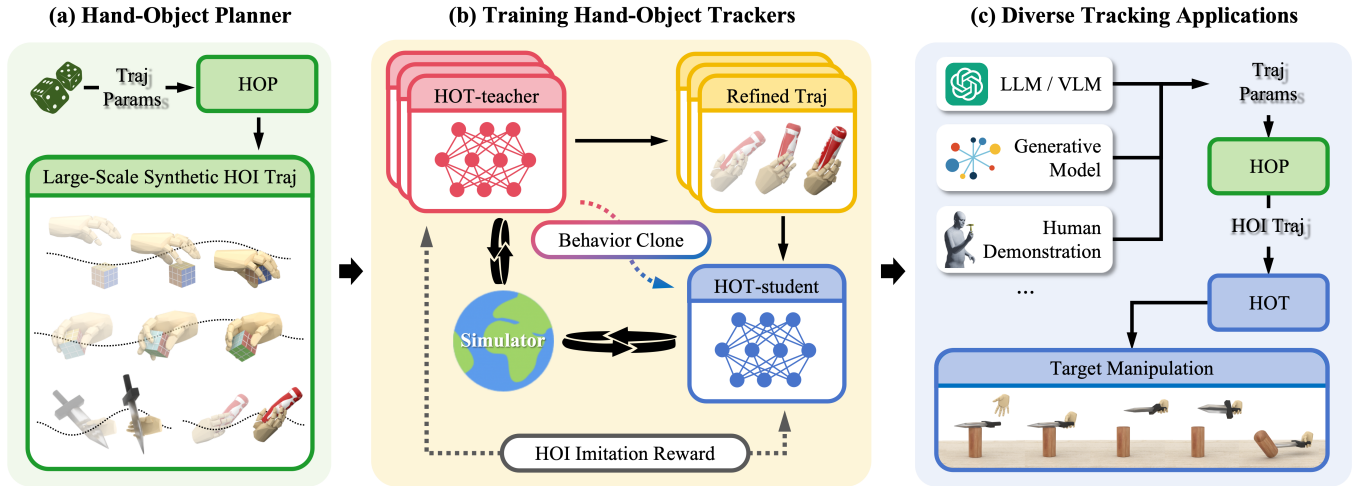


Fig. 2. Our system learns generalizable hand-object tracking from synthetic data. (a) **HOP** synthesizes manipulation trajectories for meta-skills. (b) **HOT** is trained through a two-stage teacher-student framework using reinforcement learning with a unified HOI imitation reward, enabling robust tracking of the target HOI trajectories. (c) **At inference**, the system can accept high-level waypoints from language models, generative models, or human data, which HOP converts into trajectories for HOT to track, enabling diverse applications.

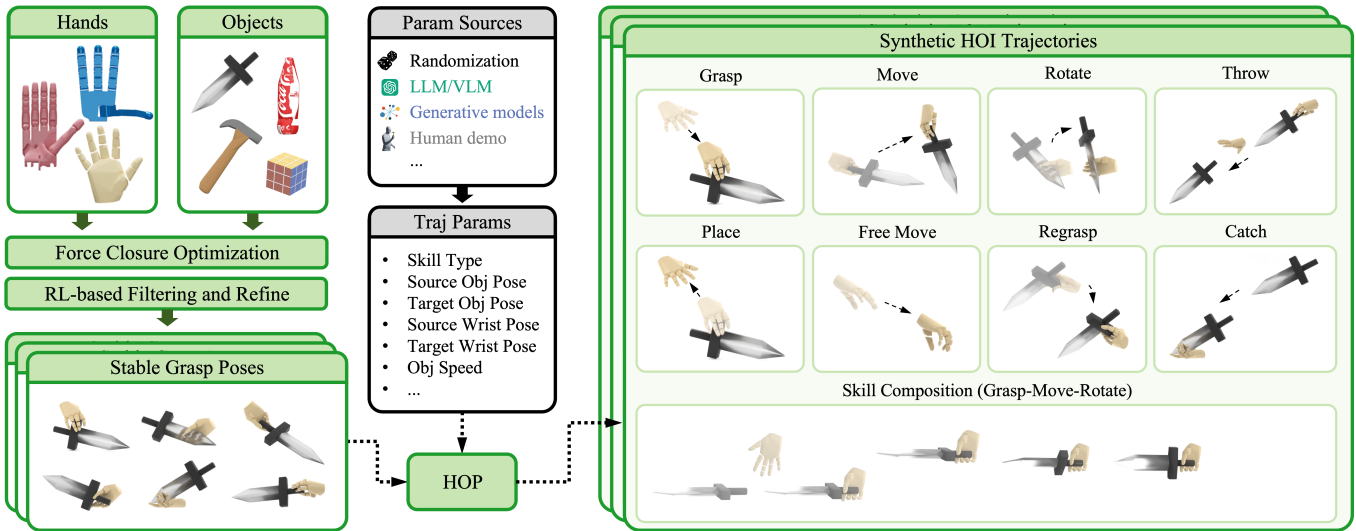


Fig. 3. HOP synthesizes manipulation trajectories from grasp poses generated by force-closure optimization and refined by RL. Its grammar-based approach supports eight composable meta-skills, offering multi-source parameter control via randomization, LLM/VLM instructions, or from human demonstrations. The system naturally generalizes across diverse hands and objects for scalable data coverage.

Free Move. Free Move represents the hand’s ability to navigate freely in space without object interaction. To generate this data, we randomly select two poses in the operational space as the wrist’s initial and final poses. We then randomly generate two sets of finger configurations to form complete initial and final hand states. The trajectory is obtained through interpolation between these states.

Grasp. The Grasp skill involves grasping objects placed on the ground. First, we determine the set of stable object poses for a given object through physics simulation by randomly dropping objects and recording their resting poses, denoted as $\mathcal{H} = \{\mathbf{h}_1, \mathbf{h}_2, \dots, \mathbf{h}_K\}$, where

each $\mathbf{h} = [\mathbf{T}^o, \mathbf{R}^o]$ represents a stable object pose. To generate a grasp trajectory, we sample a grasp configuration \mathbf{g} from \mathcal{G} and a stable object pose \mathbf{h} from \mathcal{H} , then transform \mathbf{g} to align the object pose with \mathbf{h} , obtaining \mathbf{g}^{end} . We reject and resample \mathbf{g}^{end} if any hand keypoints penetrate the ground plane; otherwise, keep it as the grasping frame. To generate the initial state \mathbf{g}^{init} , we compute the vector \mathbf{v} from object center to the first joint of the index finger, randomly sample the initial hand position within a cone centered along \mathbf{v} , set all hand joint angles to zero, while keeping other parameters identical

to \mathbf{g}^{end} . Finally, we generate the continuous grasp trajectory by interpolating between \mathbf{g}^{init} and \mathbf{g}^{end} .

Place. Place represents the inverse operation of Grasp, where an object is stably positioned on the surface followed by hand release. We efficiently generate Place demonstrations by time-reversing the Grasp trajectories.

Move. Move represents moving the objects through space while maintaining a fixed grasp configuration. To synthesize these demonstrations, we first randomly select a grasp configuration \mathbf{g} from \mathcal{G} . We then generate random initial and final object poses within the operational space and create an object trajectory through interpolation. The wrist pose is subsequently aligned with the object trajectory at each timestep, maintaining the constant relative grasp configuration throughout the motion. Notably, we also generate Move trajectories starting from the final frame of Grasp demonstrations or ending at the initial frame of Place demonstrations to ensure smooth cross-skill transitions.

Rotate. Rotate demonstrates in-hand manipulation where the object is rotated while maintaining a fixed wrist pose. We provide details for generating general Rotate data in the appendix. However, due to its difficulty and lengthy training requirements, we propose a simplified version that balances practical value with complexity. First, we define a rotatable region and rotation axis for each object, such as the hammer handle. If a grasp configuration \mathbf{g}^1 from \mathcal{G} contacts the object's rotatable region, we designate it as the first keyframe. We then rotate the object a random degree around the defined axis to create the second keyframe, and continue this process for subsequent keyframes. To accommodate large state changes, we replicate each \mathbf{g}_i for N_i frames, with N_i scaled by the magnitude of the state difference. This provides a sufficient learning buffer for the policy. The resulting demonstration is:

$$\underbrace{\{\mathbf{g}_1, \dots, \mathbf{g}_1\}}_{N_1}, \underbrace{\{\mathbf{g}_2, \dots, \mathbf{g}_2\}}_{N_2}, \dots, \underbrace{\{\mathbf{g}_k, \dots, \mathbf{g}_k\}}_{N_k}, \quad (2)$$

3.2 Hand-Object Tracker

The final goal is to train a Hand-Object Tracker (HOT) that can not only track various meta-skill demonstrations but also track composite long-horizon sequences. We employ reinforcement learning in physical simulation with a unified imitation reward to learn from synthetic demonstrations generated by Sec. 3.1. We condition the controller on target hand-object states, enabling the controller to accomplish tasks of varying duration and semantic complexity through tracking. Further, we pursue improved tracking performance through a two-stage training strategy based on the teacher-student framework [Luo et al. 2023; Xu et al. 2025].

3.2.1 HOT Structure.

Control Scheme. We employ a single policy that outputs controls for both the hand's native joints (e.g., MANO's 45 DoFs) and the wrist's 6-DoF pose, which is essential for dynamic tasks. To enhance generalization, we leverage the translational invariance of manipulation: the relative control strategy should be location-agnostic. Consequently, our policy is trained to output residual adjustments for the wrist, ensuring consistent skill execution across the workspace.



Fig. 4. HOT is able to track and refine imperfect synthetic HOI demonstrations. **Left:** sword grasp. **Right:** bottle regrasp.

Policy Formulation. The HOT is formulated as a policy parameterized by a MLP network. The output of the policy, i.e., the action, is parameterized as a Gaussian distribution

$$\mathbf{a}_t \sim \mathcal{N}(\boldsymbol{\phi}_\pi(\mathbf{h}_t), \Sigma_\pi), \quad (3)$$

where $\boldsymbol{\phi}_\pi$ is a three-layer MLP that maps input \mathbf{h}_t to action means. The variances Σ_π are set to non-zero constants during training for exploration and 0 during testing for stability. The action \mathbf{a}_t consists of residual 6-DoF wrist pose $\boldsymbol{\delta}_t^{wrist}$ and target finger joint rotations \mathbf{a}_t^{finger} . For wrist pose control, we employ an incremental control scheme where the target wrist 6-DoF is updated as $\mathbf{a}_t^{wrist} = \mathbf{a}_{t-1}^{wrist} + \boldsymbol{\delta}_t^{wrist}$. For finger joints, we apply direct position control using \mathbf{a}_t^{finger} as target DoF. These targets are converted to torque commands through PD controllers.

Policy Input. The observation of the HOT policy is

$$\mathbf{h}_t = \{\mathbf{s}_t, \hat{\mathbf{s}}_{t+1}^{goal}\} \quad (4)$$

where $\mathbf{s}_t = \{\mathbf{s}_t^{hand}, \mathbf{s}_t^{obj}\}$ is the environmental observation, constitutes of current hand state \mathbf{s}_t^{hand} and object state \mathbf{s}_t^{obj} in the simulation environment. The hand state \mathbf{s}_t^{hand} encompasses global wrist position \mathbf{s}_t^{wp} and rotation \mathbf{s}_t^{wr} , finger joint angles \mathbf{s}_t^{fr} and angular velocity \mathbf{s}_t^{frov} , finger joint positions \mathbf{s}_t^{fp} and velocity \mathbf{s}_t^{fppv} , and fingertip force sensors \mathbf{s}_t^{fs} . The object state \mathbf{s}_t^{obj} consists of the object position \mathbf{s}_t^{op} , rotation \mathbf{s}_t^{or} , velocity \mathbf{s}_t^{opv} , angular velocity \mathbf{s}_t^{orv} , and the positions of keypoints on the object surface \mathbf{s}_t^{okp} . $\hat{\mathbf{s}}_{t+1}^{goal}$ denotes the goal state for the subsequent time step, which encompasses multiple components:

$$\hat{\mathbf{s}}_{t+1}^{goal} = \{\hat{\mathbf{s}}_{t+1}^{wr}, \hat{\mathbf{s}}_{t+1}^{wp}, \hat{\mathbf{s}}_{t+1}^{wvp}, \hat{\mathbf{s}}_{t+1}^{fr}, \hat{\mathbf{s}}_{t+1}^{fp}, \hat{\mathbf{s}}_{t+1}^{or}\} \quad (5)$$

These symbols follow the similar notation as above, with the goal state values extracted from the next frame of reference data. Notably, all positional measurements (except for global wrist position) are transformed into a local coordinate frame defined by the wrist coordinate.

3.2.2 Training the Hand-Object Tracker. As illustrated in Fig. 2(b), we train the Hand-Object Tracker (HOT) using a two-stage reinforcement learning framework guided by synthetic demonstration trajectories with unified HOI imitation rewards. The training process begins by sampling a trajectory clip $\tau = \{\hat{\mathbf{s}}_t\}_{t=0}^T$ from the HOP-generated dataset (Sec. 3.1). The hand-object system is initialized using the first frame of τ . At each timestep, the policy outputs

actions (Eq. 3) that are executed in simulation, after which an imitation reward $r_t = f(\mathbf{s}_{t+1}, \hat{\mathbf{s}}_{t+1})$ (Sec. 3.2.3) is computed by comparing the current state with the reference. Network parameters ϕ_π are optimized using PPO [Schulman et al. 2017], and the process repeats until convergence.

Teacher-Student Training Framework. While effective for individual skills, using a single policy to learn diverse skills or object categories faces scalability limitations. The primary challenge arises from physical implausibilities in synthetic data, which require extensive sampling to identify feasible solutions for each instance. As the dataset expands, sampling density per trajectory decreases, adversely affecting convergence. To overcome this bottleneck, we adopt a two-stage teacher-student distillation framework [He et al. 2024; Luo et al. 2023]. In the first stage, we train specialized teacher policies for different meta-skill category (or for different object). In the second stage, a unified student policy learns to assimilate all skills simultaneously, using the teacher policies for both online data refinement and action guidance through behavior cloning [Juravsky et al. 2024; Xu et al. 2025]. This approach significantly enhances training efficiency and final performance, enabling robust learning across the full spectrum of manipulation skills.

Domain Randomization Curriculum. We apply several domain randomization [Peng et al. 2018; Tobin et al. 2017; Yu et al. 2025] techniques to enhance policy robustness. During training, we independently randomize the following aspects: (1) applying random perturbation forces to the object when Move data is sampled; (2) randomizing the object’s physical properties, including its geometry size, density, restitution, and friction coefficients; and (3) adding perturbations to the initial hand-object states. The intensity of these randomization factors follows a curriculum, starting from a low initial magnitude and progressively increasing until it reaches a predefined upper bound.

Adaptive Sampling. Due to the varying difficulty levels across our large-scale dataset, we adopted a reweighting technique [Yu et al. 2025] to ensure balanced learning. This approach dynamically adjusts the sampling probability of reference trajectories during training, providing more learning opportunities for challenging samples. The detailed implementation is described in the appendix.

3.2.3 Unified Hand-Object Imitation Reward. Inspired by [Wang et al. 2023a, 2025], we design a unified imitation reward to learn manipulation from demonstrations. The reward combines complementary components multiplicatively:

$$r_t = r_t^{\text{hand}} * r_t^{\text{wrist}} * r_t^{\text{object}} * r_t^{\text{interact}} * r_t^{\text{contact}}, \quad (6)$$

where r_t^{hand} and r_t^{wrist} are the hand and wrist tracking reward that encourages following demonstrated global hand motion trajectories, r_t^{object} captures object global motion, r_t^{interact} highlight hand-object relative motion, and r_t^{contact} encourages correct per-frame contact status. Given the considerable degradation in our demonstration data, we deliberately exclude velocity terms from the imitation objectives to ensure robust learning. Details regarding the calculation of sub-rewards can be found in the appendix.

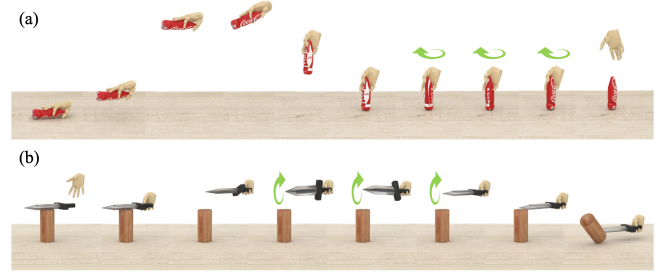


Fig. 5. Synthesizing and tracking complex HOI trajectories. (a): Grasp-Move-Rotate-Place. (b): Grasp-Move-Rotate-Move.

4 Experiment

4.1 Experimental Settings

All experiments are conducted in Isaac Gym [Makoviychuk et al. 2021] using a single RTX 4090 GPU. Teacher policies for individual skills are trained for 30,000 epochs, while multi-skill and multi-object distillation processes are trained for 20,000 epochs. The simulation and PD controller operate at 120 Hz, with policy executed at 60 Hz. Additional hyperparameters and simulation settings are provided in the appendix.

We apply four metrics for evaluation: (1) Object position error (E_{op}), (2) Object rotation error (E_{or}), (3) Mean per-joint position error for hand (E_h), and (4) Success Rate (SR) computed as the average successful execution across all frames. E_{op} and E_h are measured in centimeters, while E_{or} is measured in degrees. Results are averaged over 5000 test iterations per sequence.

4.2 Meta-Skill Tracking Performance

We evaluate meta-skill tracking performance using the MANO hand model [Romero et al. 2022] on a diverse dataset comprising four object categories: hammer, sword, cube, and bottle. For each category, we generate roughly 20 distinct grasp configurations. From these grasps, our data generation pipeline produces approximately 1,000 meta-skill demonstrations per skill for training, and a separate set of 100 demonstrations per skill for testing. All motion data is captured at 60 fps. A dedicated teacher HOT is trained for each meta-skill to perform the tracking evaluation.

We compare our method against three baseline approaches: (1) an *Open-Loop* controller that directly drives a PD controller using joint rotations from reference demonstrations; (2) *SkillMimic* [Wang et al. 2025], an HOI imitation method that observes only the 6D object pose without shape information; and (3) a reimplemented *DexGen-style* variant [Yin et al. 2025], which perceives object states indirectly through PD controller errors rather than via direct state observation. Implementation details are provided in the appendix.

Quantitative results are summarized in Tab. 1. The Open-Loop baseline performs well in Place and Move tasks, as these skills either maintain a stable force-closure grasp (Move) or involve a simple object release onto a surface (Place). However, for skills such as Grasp—where synthetic references may contain physical inconsistencies (see Fig. 4)—the open-loop strategy often fails. In contrast,

Table 1. HOI Tracking Performance on Meta Skills.

Method	SR \uparrow	$E_{op}\downarrow$	$E_{or}\downarrow$	$E_h\downarrow$	SR \uparrow	$E_{op}\downarrow$	$E_{or}\downarrow$	$E_h\downarrow$	SR \uparrow	$E_{op}\downarrow$	$E_{or}\downarrow$	$E_h\downarrow$	SR \uparrow	$E_{op}\downarrow$	$E_{or}\downarrow$	$E_h\downarrow$
	Grasp				Place				Move				Rotate			
Open-Loop	34.22%	6.05	27.26	2.50	91.45%	1.93	22.78	1.99	82.04%	4.33	24.88	4.84	0.0%	1.31	72.62	0.99
SkillMimic [Wang et al. 2025]	56.98%	6.15	21.99	5.69	87.92%	2.42	14.92	4.61	88.04%	4.56	17.46	5.70	17.52%	8.41	86.51	36.36
DexGen-var [Yin et al. 2025]	4.77%	7.81	13.15	5.83	78.98%	3.00	19.91	4.44	78.73%	8.06	28.63	5.10	0.0%	2.23	72.50	2.83
HOT (Teacher)	85.97%	3.80	11.76	4.32	94.33%	1.24	9.88	3.14	98.87%	2.01	9.83	4.50	56.23%	2.38	44.96	2.57
Method	Throw				Catch				Regrasp				Avg.			
	SR \uparrow	$E_{op}\downarrow$	$E_{or}\downarrow$	$E_k\downarrow$	SR \uparrow	$E_{op}\downarrow$	$E_{or}\downarrow$	$E_k\downarrow$	SR \uparrow	$E_{op}\downarrow$	$E_{or}\downarrow$	$E_k\downarrow$	SR \uparrow	$E_{op}\downarrow$	$E_{or}\downarrow$	$E_k\downarrow$
Open-Loop	9.22%	20.20	91.64	2.56	27.88%	13.04	89.30	1.51	0.0%	21.89	71.84	1.31	34.97%	9.82	57.19	2.24
SkillMimic [Wang et al. 2025]	0.40%	45.41	97.86	46.43	64.79%	6.96	53.65	4.31	0.0%	7.54	64.28	4.18	43.15%	11.45	51.24	15.48
DexGen-var [Yin et al. 2025]	0.62%	41.19	90.00	44.72	35.94%	12.13	85.61	4.35	0.0%	10.47	58.29	4.92	26.94%	11.86	52.71	10.70
HOT (Teacher)	91.94%	15.04	35.27	8.34	83.59%	3.34	45.00	2.67	81.92%	1.56	14.05	2.90	84.69%	4.20	24.39	4.06

Table 2. HOI Tracking Performance on Long-Horizon Task.

Dataset	SR \uparrow	$E_{op}\downarrow$	$E_{or}\downarrow$	$E_k\downarrow$
Bottle (<i>Grasp–Move–Place</i>)	58.54%	9.00	34.77	4.94
Box (<i>Grasp–Move–Place</i>)	84.21%	5.69	34.45	4.69
Hammer (<i>Grasp–Move–Place</i>)	57.91%	9.40	38.33	5.37
Sword (<i>Grasp–Move–Place</i>)	68.42%	10.40	33.31	4.80
Average	67.27%	8.62	35.22	4.95

Table 3. Generalized HOI Tracking Performance on GRAB.

Dataset	SR-grasp \uparrow	SR \uparrow	$E_{op}\downarrow$	$E_{or}\downarrow$	$E_k\downarrow$
GRAB-Apple	3/3	3/3	1.64	46.43	4.82
GRAB-Bowl	3/3	3/3	2.59	49.22	5.03
GRAB-Cup	3/3	1/3	2.58	15.48	9.56
GRAB-Hammer	2/3	2/3	5.89	36.36	5.75
GRAB-Stanfordbunny	1/3	1/3	9.51	68.07	5.02
GRAB-Stapler	2/3	2/3	4.26	29.59	5.62
GRAB-Train	3/3	2/3	12.81	42.74	6.47
GRAB-Torus_large	1/2	0/2	24.77	89.07	11.71
GRAB-Waterbottle	3/4	3/4	4.38	19.40	4.33
GRAB-Wineglass	2/4	1/4	38.13	44.55	6.10
Average	23/31	18/31	10.66	44.09	6.44

Table 4. Ablation on Reward Design.

Reward	Grasp				Place			
	SR \uparrow	$E_{op}\downarrow$	$E_{or}\downarrow$	$E_h\downarrow$	SR \uparrow	$E_{op}\downarrow$	$E_{or}\downarrow$	$E_h\downarrow$
w/o $r^{contact}$	0.00%	6.73	1.75	9.11	95.99%	1.68	9.83	4.86
w/o $r^{interact}$	72.29%	3.13	20.61	7.15	96.06%	1.83	13.03	4.57
w/o r^{wrist}	77.93%	2.07	14.48	5.55	55.61%	1.20	12.75	3.04
w/o r^{object}	91.25%	2.20	38.99	5.98	99.79%	1.72	14.43	3.23
w/o r^{hand}	74.70%	2.96	20.32	4.73	98.02%	1.72	8.85	3.35
HOT (full)	94.44%	2.10	10.27	3.63	98.18%	1.04	9.05	2.65

by using the same imperfect references within a reinforcement imitation learning framework, our HOT yields high success rates and low tracking errors across most skills.

Both SkillMimic [Wang et al. 2025] and DexGen-var [Yin et al. 2025] perform substantially worse than HOT. DexGen-var struggles with precise object tracking due to its lack of direct object state observation. The low performance of SkillMimic further underscores

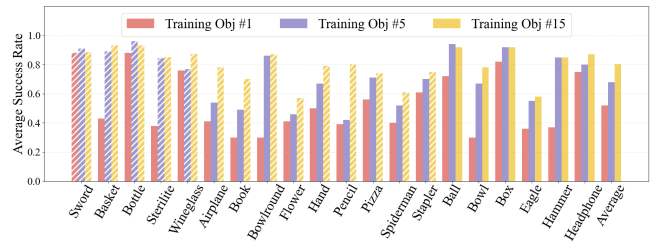


Fig. 6. Evaluation of HOT’s object generalization performance. The dashed bars denote objects present in the training set, while the undashed bars represent objects unseen during training.

the importance of our design choices—including reward shaping, observation localization, geometry perception, residual action, and adaptive sampling—in achieving robust HOI tracking performance.

4.3 Complex Long-Horizon HOI Trajectories

To evaluate scalability to complex behaviors, we use HOP to synthesize HOI demonstration for composite long-horizon tasks, such as Catch–Rotate–Move and Grasp–Move–Place–Rotate. A separate HOT policy is trained for each composite task, all of which converged successfully and demonstrated robust generalization to novel instances. Tracking results are shown in Fig. 1(b) and Fig. 5, affirming the method’s capacity for synthesizing and tracking complex multi-skill HOI trajectories.

4.4 Generalized HOI Tracking Performance

To develop a HOT capable of generalizing across object shapes and long-horizon trajectories, we construct a meta-skill training dataset consisting of grasp, move, and place sequences over 15 diverse objects. For each object, a specialized teacher HOT is trained. These teachers are then distilled into a unified student HOT. As shown in Fig. 6, we evaluate object generalization capability by comparing HOT trained on 1, 5, and 15 objects, reporting the average tracking success rates for Grasp, Move, and Place across 20 test objects. The results demonstrate that our method converges stably under multi-object joint training and generalizes effectively to unseen objects, with performance improving as training object diversity increases.

The trajectory generalization performance is evaluated on procedurally generated grasp–move–place trajectories. As shown in



Fig. 7. Versatile applications of the HOP-HOT system.

Tab. 2, the student HOP achieves strong performance in these long-horizon tasks, despite having never been explicitly trained on such composite sequences.

We further validate generalized tracking performance on real-world data using segmented trajectories from the GRAB dataset [Taheri et al. 2020], where trajectories are refined by HOP for retargeting and improved physical plausibility (See the appendix for details). Qualitative and quantitative results are shown in Fig. 1(c), Fig. 7(a), and Tab. 3. Here, SR-grasp measures the success rate of achieving a stable grasp, while SR evaluates the success rate of the complete tracking. Notably, HOP achieves effective zero-shot tracking on real hand-object interactions despite being trained purely on synthetic data, demonstrating its potential to overcome the data bottleneck in general dexterous manipulation.

4.5 Ablation Study

We conduct ablation studies to evaluate the impact of key design choices. First, we analyze the reward function design using motion clips of three meta-skills (Grasp, Move, Place) on the bottle object, with 1000 training and 100 testing clips per skill. As shown in Tab. 4, each reward term contributes noticeably to performance, and the complete reward formulation yields the best overall results. We present more ablation studies in the appendix.

4.6 Following Text Instructions

Our framework supports manipulation from natural language instructions through multiple complementary approaches. The typical

pipeline uses a Vision-Language Model (VLM) for high-level semantic planning. The VLM takes as input: the object’s initial 6D pose, a set of feasible wrist poses corresponding to stable grasp configurations, the initial wrist pose, the target object position, an image of current environment, and a natural-language task description. It outputs a structured plan containing: (1) sparse 6D waypoints for the wrist at key states (start, grasp, release, end), (2) a selected grasp pose, and (3) binary flags indicating grasp and release events. We also explore an alternative that uses Text2HOI [Cha et al. 2024] to generate wrist trajectories directly from language. In both cases, we apply trajectory smoothing and Bayesian interpolation between keyframes to ensure smooth motions. The resulting wrist path is combined with the chosen grasp pose using the procedure in Sec. 3.1.3 to form a complete hand-object demonstration. This is then tracked by our distilled student HOP, demonstrating end-to-end execution of language-guided manipulation. Fig. 1(d) and Fig. 7(b,c) shows representative results.

5 Conclusion

We presented a system for generalizable dexterous manipulation that combines synthetic data generation with tracking-based control. Our approach consists of HOP, a scalable framework for synthesizing hand-object trajectories across diverse meta-skills, and HOP, a tracking policy trained via reinforcement imitation learning on such data. The resulting controller demonstrates effective generalization to unseen objects, long-horizon tasks, and even real-world human-object motion data. By functioning effectively without human demonstrations while remaining compatible with them, our method offers a flexible, scalable, and powerful foundation for future work on general-purpose dexterous manipulation.

References

- Josh Achiam, Steven Adler, Sandhini Agarwal, Lama Ahmad, Ilge Akkaya, Florencia Leoni Aleman, Diogo Almeida, Janko Altenschmidt, Sam Altman, Shyamal Anadkat, et al. 2023. Gpt-4 technical report. *arXiv preprint arXiv:2303.08774* (2023).
- Arthur Allshire, Mayank Mittal, Varun Lodaya, Viktor Makoviychuk, Denys Makoviychuk, Felix Widmaier, Manuel Wüthrich, Stefan Bauer, Ankur Handa, and Animesh Garg. 2022. Transferring dexterous manipulation from gpu simulation to a remote real-world trifinger. In *2022 IEEE/RSJ International Conference on Intelligent Robots and Systems (IROS)*. IEEE, 11802–11809.
- OpenAI: Marcin Andrychowicz, Bowen Baker, Maciek Chociej, Rafal Jozefowicz, Bob McGrew, Jakob Pachocki, Arthur Petron, Matthias Plappert, Glenn Powell, Alex Ray, et al. 2020. Learning dexterous in-hand manipulation. *The International Journal of Robotics Research* 39, 1 (2020), 3–20.
- Prithviraj Banerjee, Sindi Shkodrani, Pierre Moulon, Shreyas Hampali, Fan Zhang, Jade Fountain, Edward Miller, Selen Basol, Richard Newcombe, Robert Wang, et al. 2024. Introducing HOT3D: An Egocentric Dataset for 3D Hand and Object Tracking. *arXiv preprint arXiv:2406.09598* (2024).
- Zhe Cao, Ilija Radosavovic, Angjoo Kanazawa, and Jitendra Malik. 2021. Reconstructing hand-object interactions in the wild. In *Proceedings of the IEEE/CVF International Conference on Computer Vision*. 12417–12426.
- Junuk Cha, Jihyeon Kim, Jae Shin Yoon, and Seungryul Baek. 2024. Text2hoi: Text-guided 3d motion generation for hand-object interaction. In *Proceedings of the IEEE/CVF Conference on Computer Vision and Pattern Recognition*. 1577–1585.
- Yu-Wei Chao, Wei Yang, Yu Xiang, Pavlo Molchanov, Ankur Handa, Jonathan Tremblay, Yashraj S Narang, Karl Van Wyk, Umar Iqbal, Stan Birchfield, et al. 2021. DexYCB: A benchmark for capturing hand grasping of objects. In *Proceedings of the IEEE/CVF Conference on Computer Vision and Pattern Recognition*. 9044–9053.
- Yuanpei Chen, Yiran Geng, Fangwei Zhong, Jiaming Ji, Jiechuang Jiang, Zongqing Lu, Hao Dong, and Yaodong Yang. 2023a. Bi-dexhands: Towards human-level bimanual dexterous manipulation. *IEEE Transactions on Pattern Analysis and Machine Intelligence* (2023).
- Yuanpei Chen, Chen Wang, Li Fei-Fei, and C Karen Liu. 2023b. Sequential dexterity: Chaining dexterous policies for long-horizon manipulation. *arXiv preprint*

- arXiv:2309.00987 (2023).
- Yuanpei Chen, Chen Wang, Yaodong Yang, and C Karen Liu. 2024. Object-centric dexterous manipulation from human motion data. *arXiv preprint arXiv:2411.04005* (2024).
- Xuxin Cheng, Jialong Li, Shiqi Yang, Ge Yang, and Xiaolong Wang. 2024. Open-television: Teleoperation with immersive active visual feedback. *arXiv preprint arXiv:2407.01512* (2024).
- Shadow Robot Developers. 2005. Shadow Robot. <https://www.shadowrobot.com/dexterous-hand-series/> (2005).
- Zicong Fan, Omid Taheri, Dimitrios Tzionas, Muhammed Kocabas, Manuel Kaufmann, Michael J Black, and Otmar Hilliges. 2023. ARCTIC: A Dataset for Dexterous Bimanual Hand-Object Manipulation. In *Proceedings of the IEEE/CVF Conference on Computer Vision and Pattern Recognition*. 12943–12954.
- Hao-Shu Fang, Chenxi Wang, Hongjie Fang, Minghao Gou, Jirong Liu, Hengxu Yan, Wenhai Liu, Yichen Xie, and Cewu Lu. 2023. Anygrasp: Robust and efficient grasp perception in spatial and temporal domains. *IEEE Transactions on Robotics* (2023).
- Zipeng Fu, Qingqing Zhao, Qi Wu, Gordon Wetzstein, and Chelsea Finn. 2024. HumanPlus: Humanoid Shadowing and Imitation from Humans. *arXiv preprint arXiv:2406.10454* (2024).
- Jensen Gao, Annie Xie, Ted Xiao, Chelsea Finn, and Dorsa Sadigh. 2024. Efficient Data Collection for Robotic Manipulation via Compositional Generalization. *arXiv preprint arXiv:2403.05110* (2024).
- Caelan Garrett, Ajay Mandelkar, Bowen Wen, and Dieter Fox. 2024. SkillMimicGen: Automated Demonstration Generation for Efficient Skill Learning and Deployment. *arXiv preprint arXiv:2410.18907* (2024).
- Yana Hasson, Gul Varol, Dimitrios Tzionas, Igor Kalevtykh, Michael J Black, Ivan Laptev, and Cordelia Schmid. 2019. Learning joint reconstruction of hands and manipulated objects. In *Proceedings of the IEEE/CVF conference on computer vision and pattern recognition*. 11807–11816.
- Tairan He, Zhengyi Luo, Xialin He, Wenli Xiao, Chong Zhang, Weinan Zhang, Kris Kitani, Changliu Liu, and Guanya Shi. 2024. OmniH2O: Universal and Dexterous Human-to-Humanoid Whole-Body Teleoperation and Learning. *arXiv preprint arXiv:2406.08858* (2024).
- Binghao Huang, Yuanpei Chen, Tianyu Wang, Yuzhe Qin, Yaodong Yang, Nikolay Atanasov, and Xiaolong Wang. 2023. Dynamic handover: Throw and catch with bimanual hands. *arXiv preprint arXiv:2309.05655* (2023).
- Zhenyu Jiang, Yuqi Xie, Kevin Lin, Zhenjia Xu, Weikang Wan, Ajay Mandelkar, Linxi Fan, and Yuke Zhu. 2024. DexMimicGen: Automated Data Generation for Bimanual Dexterous Manipulation via Imitation Learning. *arXiv preprint arXiv:2410.24185* (2024).
- Jordan Juravsky, Yunrong Guo, Sanja Fidler, and Xue Bin Peng. 2024. Superpadl: Scaling language-directed physics-based control with progressive supervised distillation. In *ACM SIGGRAPH 2024 Conference Papers*. 1–11.
- Jeonghwan Kim, Jisoo Kim, Jeonghyeon Na, and Hanbyul Joo. 2024. ParaHome: Parameterizing Everyday Home Activities Towards 3D Generative Modeling of Human-Object Interactions. *arXiv preprint arXiv:2401.10232* (2024).
- Kailin Li, Puhao Li, Tengyu Liu, Yuyang Li, and Siyuan Huang. 2025. Maniptrans: Efficient dexterous bimanual manipulation transfer via residual learning. In *Proceedings of the Computer Vision and Pattern Recognition Conference*. 6991–7003.
- Tengyu Liu, Zeyu Liu, Ziyuan Jiao, Yixin Zhu, and Song-Chun Zhu. 2021. Synthesizing diverse and physically stable grasps with arbitrary hand structures using differentiable force closure estimator. *IEEE Robotics and Automation Letters* 7, 1 (2021), 470–477.
- Xueyi Liu, Jianbieke Adalibieke, Qianwei Han, Yuzhe Qin, and Li Yi. 2025. DexTrack: Towards Generalizable Neural Tracking Control for Dexterous Manipulation from Human References. *arXiv preprint arXiv:2502.09614* (2025).
- Zhengyi Luo, Jinkun Cao, Kris Kitani, Weipeng Xu, et al. 2023. Perpetual humanoid control for real-time simulated avatars. In *Proceedings of the IEEE/CVF International Conference on Computer Vision*. 10895–10904.
- Viktor Makoviychuk, Lukasz Wawrzyniak, Yunrong Guo, Michelle Lu, Kier Storey, Miles Macklin, David Hoeller, Nikita Rudin, Arthur Allshire, Ankur Handa, and Gavriel State. 2021. Isaac Gym: High Performance GPU Based Physics Simulation For Robot Learning. In *Thirty-fifth Conference on Neural Information Processing Systems Datasets and Benchmarks Track (Round 2)*. <https://openreview.net/forum?id=fgFBtYgJQX>.
- Ajay Mandelkar, Soroush Nasiriany, Bowen Wen, Iretyayo Akinola, Yashraj Narang, Linxi Fan, Yuke Zhu, and Dieter Fox. 2023. Mimicgen: A data generation system for scalable robot learning using human demonstrations. *arXiv preprint arXiv:2310.17596* (2023).
- Andrew T Miller and Peter K Allen. 2004. Graspit! a versatile simulator for robotic grasping. *IEEE Robotics & Automation Magazine* 11, 4 (2004), 110–122.
- Xue Bin Peng, Marcin Andrychowicz, Wojciech Zaremba, and Pieter Abbeel. 2018. Sim-to-real transfer of robotic control with dynamics randomization. In *2018 IEEE international conference on robotics and automation (ICRA)*. IEEE, 3803–3810.
- Wilbert Pumacay, Ishika Singh, Jiafei Duan, Ranjay Krishna, Jesse Thomason, and Dieter Fox. 2024. The colosseum: A benchmark for evaluating generalization for robotic manipulation. *arXiv preprint arXiv:2402.08191* (2024).
- Aravind Rajeswaran, Vikash Kumar, Abhishek Gupta, Giulia Vezzani, John Schulman, Emanuel Todorov, and Sergey Levine. 2018. Learning Complex Dexterous Manipulation with Deep Reinforcement Learning and Demonstrations. *Robotics: Science and Systems XIV* (2018).
- Wonik Robotics. 2013. Allegro Hand. <https://www.allegrohand.com/> (2013).
- Javier Romero, Dimitrios Tzionas, and Michael J Black. 2017. Embodied Hands: Modeling and Capturing Hands and Bodies Together. *ACM Transactions on Graphics* 36, 6 (2017).
- Javier Romero, Dimitrios Tzionas, and Michael J Black. 2022. Embodied hands: Modeling and capturing hands and bodies together. *arXiv preprint arXiv:2201.02610* (2022).
- John Schulman, Filip Wolski, Prafulla Dhariwal, Alec Radford, and Oleg Klimov. 2017. Proximal policy optimization algorithms. *arXiv preprint arXiv:1707.06347* (2017).
- Qijin She, Ruizhen Hu, Juzhan Xu, Min Liu, Kai Xu, and Hui Huang. 2022. Learning high-DOF reaching-and-grasping via dynamic representation of gripper-object interaction. *arXiv preprint arXiv:2204.13998* (2022).
- Qijin She, Shishun Zhang, Yunfan Ye, Ruizhen Hu, and Kai Xu. 2024. Learning Cross-Hand Policies of High-DOF Reaching and Grasping. In *European Conference on Computer Vision*. Springer, 269–285.
- Omid Taheri, Nima Ghorbani, Michael J. Black, and Dimitrios Tzionas. 2020. GRAB: A Dataset of Whole-Body Human Grasping of Objects. In *European Conference on Computer Vision (ECCV)*. <https://grab.is.tue.mpg.de>
- Gemini Team, Rohan Anil, Sebastian Borgeaud, Jean-Baptiste Alayrac, Jiahui Yu, Radu Soricut, Johan Schalkwyk, Andrew M Dai, Anja Hauth, Katie Millican, et al. 2023. Gemini: a family of highly capable multimodal models. *arXiv preprint arXiv:2312.11805* (2023).
- Josh Tobin, Rachel Fong, Alex Ray, Jonas Schneider, Wojciech Zaremba, and Pieter Abbeel. 2017. Domain randomization for transferring deep neural networks from simulation to the real world. In *2017 IEEE/RSJ international conference on intelligent robots and systems (IROS)*. IEEE, 23–30.
- Emanuel Todorov, Tom Erez, and Yuval Tassa. 2012. Mujoco: A physics engine for model-based control. In *2012 IEEE/RSJ international conference on intelligent robots and systems*. IEEE, 5026–5033.
- Weikang Wan, Haoran Geng, Yun Liu, Zikang Shan, Yaodong Yang, Li Yi, and He Wang. 2023. Unidexgrasp+: Improving dexterous grasping policy learning via geometry-aware curriculum and iterative generalist-specialist learning. In *Proceedings of the IEEE/CVF International Conference on Computer Vision*. 3891–3902.
- Ruicheng Wang, Jialiang Zhang, Jiayi Chen, Yinzheng Xu, Puhao Li, Tengyu Liu, and He Wang. 2023b. Dexgraspnet: A large-scale robotic dexterous grasp dataset for general objects based on simulation. In *2023 IEEE International Conference on Robotics and Automation (ICRA)*. IEEE, 11359–11366.
- Yinhui Wang, Jing Lin, Ailing Zeng, Zhengyi Luo, Jian Zhang, and Lei Zhang. 2023a. Physshoi: Physics-based imitation of dynamic human-object interaction. *arXiv preprint arXiv:2312.04393* (2023).
- Yinhui Wang, Qihan Zhao, Runyi Yu, Hok Wai Tsui, Ailing Zeng, Jing Lin, Zhengyi Luo, Jiwen Yu, Xiu Li, Qifeng Chen, et al. 2025. Skillmimic: Learning reusable basketball skills from demonstrations. In *Proceedings of the IEEE/CVF Conference on Computer Vision and Pattern Recognition*.
- Bowen Wen, Jonathan Tremblay, Valts Blukis, Stephen Tyree, Thomas Müller, Alex Evans, Dieter Fox, Jan Kautz, and Stan Birchfield. 2023. Bundlesdf: Neural 6-dof tracking and 3d reconstruction of unknown objects. In *Proceedings of the IEEE/CVF Conference on Computer Vision and Pattern Recognition*. 606–617.
- Sirui Xu, Hung Yu Ling, Yu-Xiong Wang, and Liang-Yan Gui. 2025. Intermimic: Towards universal whole-body control for physics-based human-object interactions. *arXiv preprint arXiv:2502.20390* (2025).
- Yinzheng Xu, Weikang Wan, Jialiang Zhang, Haoran Liu, Zikang Shan, Hao Shen, Ruicheng Wang, Haoran Geng, Yijia Weng, Jiayi Chen, et al. 2023. Unidexgrasp: Universal robotic dexterous grasping via learning diverse proposal generation and goal-conditioned policy. In *Proceedings of the IEEE/CVF Conference on Computer Vision and Pattern Recognition*. 4737–4746.
- Ruihan Yang, Huazhe Xu, Yi Wu, and Xiaolong Wang. 2020. Multi-task reinforcement learning with soft modularization. *Advances in Neural Information Processing Systems* 33 (2020), 4767–4777.
- Zhao-Heng Yin, Binghao Huang, Yuzhe Qin, Qifeng Chen, and Xiaolong Wang. 2023. Rotating without seeing: Towards in-hand dexterity through touch. *arXiv preprint arXiv:2303.10880* (2023).
- Zhao-Heng Yin, Changhao Wang, Luis Pineda, Francois Hogan, Krishna Bodduluri, Akash Sharma, Patrick Lancaster, Ishita Prasad, Mrinal Kalakrishnan, Jitendra Malik, et al. 2025. DexterityGen: Foundation Controller for Unprecedented Dexterity. *arXiv preprint arXiv:2502.04307* (2025).
- Runyi Yu, Yinhui Wang, Qihan Zhao, Hok Wai Tsui, Jingbo Wang, Ping Tan, and Qifeng Chen. 2025. SkillMimic-V2: Learning Robust and Generalizable Interaction Skills from Sparse and Noisy Demonstrations. *arXiv preprint arXiv:2505.02094* (2025).
- Hui Zhang, Sammy Christen, Zicong Fan, Otmar Hilliges, and Jie Song. 2024a. Grasppl: Generating grasping motions for diverse objects at scale. In *European Conference on Computer Vision*. Springer, 386–403.

Hui Zhang, Sammy Christen, Zicong Fan, Luocheng Zheng, Jemin Hwangbo, Jie Song, and Otmar Hilliges. 2024b. ArtiGrasp: Physically plausible synthesis of bi-manual dexterous grasping and articulation. In *2024 International Conference on 3D Vision (3DV)*. IEEE, 235–246.

Learning Generalizable Hand-Object Tracking from Synthetic Demonstrations

Supplementary Material

Table 5. Penetration Comparisons on Grasp Data

	Max Penetration (cm)	Avg Penetration (cm)
Raw Data	-0.92 (± 0.71)	-0.23 (± 0.13)
HOT	-0.28 (± 0.13)	-0.12 (± 0.08)

6 Additional Experiments

6.1 Evaluation on Allegro and Shadow Hands

To evaluate the general applicability of our approach across different hand morphologies, we conduct experiments on the Allegro Hand [Robotics 2013] and the Shadow Hand [Developers 2005]. For each hand model, we use HOP to generate corresponding training data for the Grasp, Move, and Place skills on a bottle object, and train a corresponding HOT policy. Quantitative results on the test set are presented in Tab. 6. As shown in the results, both Shadow and Allegro hands achieve over 80% average success rates. Notably, under identical settings, MANO demonstrates the best performance, followed by Shadow and then Allegro. This performance ranking aligns with their respective degrees of freedom (DoF): MANO has the highest DoF (45), followed by Shadow (20), and Allegro (16). Fig. 8 presents the performance of different hand models on unseen objects and long-horizon sequences, demonstrating our method’s strong adaptability to diverse hand morphologies.

6.2 Impact of Data Volume and Model Design

We investigate the impact of three key design choices in our approach through comprehensive ablation studies. First, we examine critical HOT design elements, specifically the localization and residualization of input-output representations that simplify the learning distribution (HOT w/o LR). Second, we study the effectiveness of our data augmentation strategies (HOT w/o DA). Third, we analyze how model performance scales with training data quantity.

The experiments are conducted on three fundamental meta-skills - Grasp, Move, and Place - with each skill trained using 10, 100, or 1000 demonstrations. Tab. 7 presents the quantitative results of our ablation studies. The localization and residualization of HOT input-output prove crucial for generalization, allowing the model to achieve superior performance even with limited training data. This validates our hypothesis that simplifying the input-output distribution enhances learning efficiency. Data augmentation techniques consistently boost generalization performance across all skills, while increased training data leads to proportional performance improvements, demonstrating our method’s ability to effectively utilize additional demonstrations.

6.3 Refining HOI Data Through Tracking

To quantitatively demonstrate HOT’s ability to refine imperfect reference data through tracking, we evaluate the trained HOT on bottle Grasp sequences from the test set generated by HOP, using object-hand penetration as the key metric. As shown in Tab. 5, the

original reference data contains noticeable penetrations, while the trajectories produced by HOT exhibit significantly reduced penetration, validating its capacity to correct physically implausible artifacts.

7 Detailed Sub-Rewards

The unified imitation reward combines complementary components multiplicatively:

$$r_t = r_t^{hand} * r_t^{wrist} * r_t^{object} * r_t^{interact} * r_t^{contact}, \quad (7)$$

Hand Tracking Reward:

$$r_t^{hand} = r_t^p * r_t^r, \quad (8)$$

where r_t^p denotes the finger joint position reward and r_t^r represents the finger joint rotation reward.

Wrist Tracking Reward:

$$r_t^{wrist} = r_t^{wp} * r_t^{wr}, \quad (9)$$

where r_t^{wp} denotes the wrist joint position reward and r_t^{wr} represents the wrist joint rotation reward.

Object Reward:

$$r_t^{object} = r_t^{op} * r_t^{or}, \quad (10)$$

where r_t^{op} and r_t^{or} denote the object global position and rotation rewards respectively.

Interaction Reward: $r_t^{interact}$ measures the hand-object relative motion by computing the consistency between two sets of positional vectors: from hand keypoints to object keypoints in both reference data and simulated environment, which is essential for interaction stability.

Contact Reward: r_t^c is the contact reward guided by frame-wise binary labels of hand-object contact from reference data, which is crucial for reliable grasping and releasing operations.

Formulation of Sub-Rewards: Each sub-terms follows:

$$r_t^\alpha = \exp(-\lambda^\alpha * e_{t+1}^\alpha), \quad (11)$$

where $\alpha \in \{p, r, wp, wr, op, or, interact, contact\}$, with e_{t+1}^α and λ^α denotes tracking error and weight hyperparameter, respectively. All λ^α are fixed except for $\lambda^{interact}$, which is dynamically adjusted based on the hand-object distance in reference data to increase relative motion sensitivity during object approaching phases, facilitating precise grasping.

8 Adaptive Sampling

To enhance performance on challenging examples, we dynamically adjust sampling probabilities according to sample difficulty. Specifically, for a trajectory $\tau_i = \{\hat{s}_1, \dots, \hat{s}_T\}$, we calculate its mean reward $\bar{r}_i = \frac{1}{T} \sum_{t=1}^T r_t$ as a metric of learning difficulty, where r_t is defined in Eq. 7. Based on this difficulty assessment, we assign a sampling probability p_i for trajectory τ_i using:

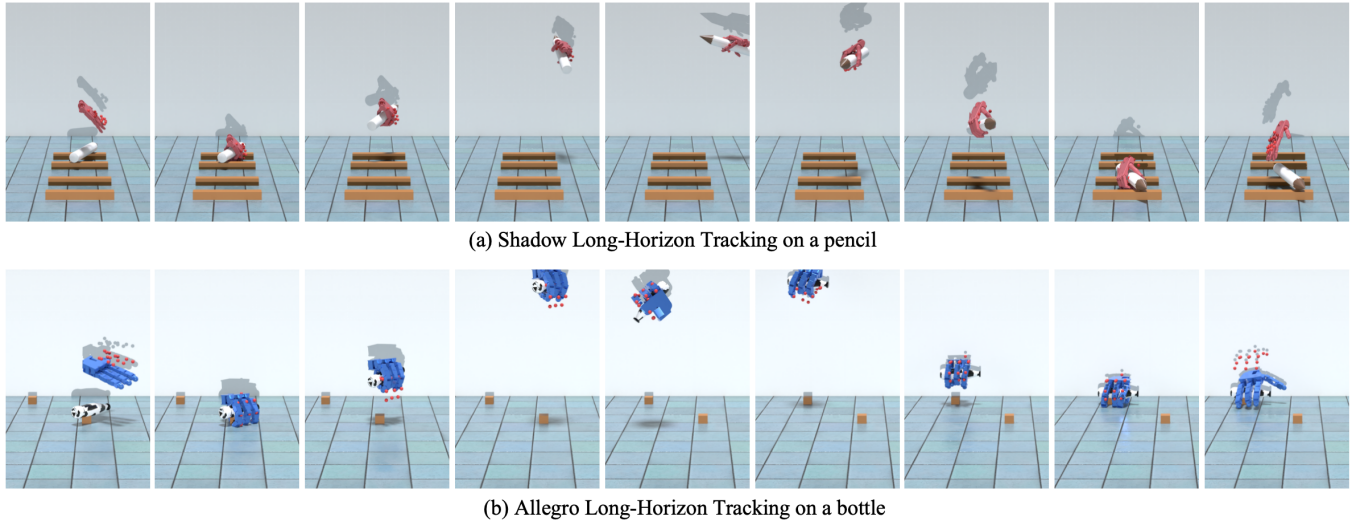


Fig. 8. HOI tracking with different robotic hands. Red dots denotes hand joint tracking targets

Table 6. Evaluation of Tracking Performance on Different Robotic Hands

Method	Grasp				Place				Move			
	SR [↑]	E_{op} [↓]	E_{or} [↓]	E_h [↓]	SR [↑]	E_{op} [↓]	E_{or} [↓]	E_h [↓]	SR [↑]	E_{op} [↓]	E_{or} [↓]	E_h [↓]
Shadow	92.58%	1.31	8.39	3.16	86.28%	1.15	6.73	2.85	95.82%	2.48	16.02	4.23
Allegro	84.80%	2.01	19.50	6.60	78.78%	1.66	13.72	5.23	89.78%	3.44	23.78	6.43
MANO	94.44%	2.10	10.27	3.63	98.18%	1.04	9.05	2.65	99.14%	1.55	7.38	3.62

Table 7. Ablation on Model Design and Data Volume.

Method	10 Clips			100 Clips			1000 Clips		
	HOT	HOT w/o LR	HOT w/o DA	HOT	HOT w/o LR	HOT w/o DA	HOT	HOT w/o LR	HOT w/o DA
Grasp	31.49%	19.41%	31.60%	73.24%	71.38%	60.22%	94.44%	64.97%	70.79%
Move	79.85%	62.04%	79.75%	97.67%	94.66%	90.89%	99.14%	95.18%	95.20%
Place	84.73%	28.12%	84.99%	100%	92.29%	100%	98.18%	100%	99.63%
Avg.	65.36%	36.52%	65.45%	90.30%	86.11%	83.37%	93.22%	86.72%	88.54%

$$p_i = \frac{e^{-\lambda_s * \bar{f}_i}}{\sum_{j=0}^{N-1} e^{-\lambda_s * \bar{f}_j}} \quad (12)$$

where N denotes the dataset size, and $\lambda_s \in [0, \infty)$ controls the balance between uniform sampling ($\lambda_s = 0$) and difficulty-prioritized sampling ($\lambda_s > 0$).

9 Implementation Details of Baseline Methods

Since neither SkillMimic [Wang et al. 2025] nor DexGen [Yin et al. 2025] provide implementation code for tracking on the MANO hand model, for comparison purposes, we modified the reward, input representations, and output formats of HOT to construct variants in the style of SkillMimic and DexGen, as detailed in Tab. 8. To

ensure fair comparison, all methods use the same data and training configurations.

10 HOP for Other Meta-Skills

Catch. Unlike Grasp, the Catch skill involves catching moving objects. To synthesize these demonstrations, we first randomly select a grasp configuration \mathbf{g} from \mathcal{G} and generate a parabolic trajectory for the object $[\mathbf{T}^o(t), \mathbf{R}^o(t)] = \text{Parabola}(t)$, $t \in [0, T]$. We then select the last frame as the grasp moment and transform \mathbf{g} to align with the object pose $[\mathbf{T}^o(T), \mathbf{R}^o(T)]$, yielding \mathbf{g}^{end} . The initial hand position and orientation are set identical to those in \mathbf{g}^{end} , while the initial joint angles are set to zero. The hand trajectory is then generated via interpolation between the initial and end hand states. The complete Catch demonstration consists of both the generated hand

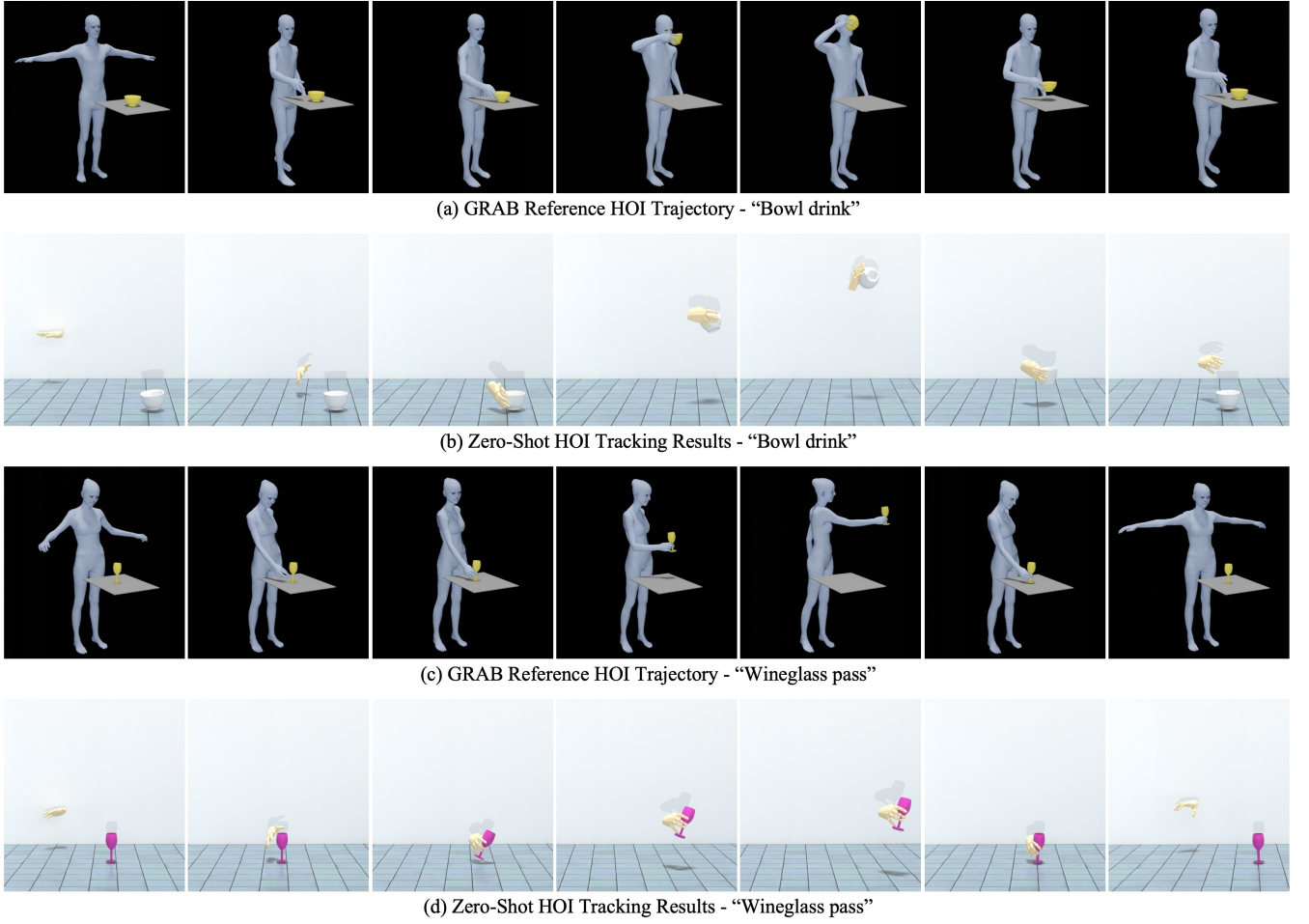


Fig. 9. Zero-shot HOI tracking on GRAB data.

Table 8. Comparisons of Implementation Details Across Methods

Feature	HOT	SkillMimic	DexGen-var
Observation	Default	No object keypoints	No object information
Reward	Default	Default	Object pose & finger DoF only
Action	Direct finger & Residual wrist	Direct action	Direct action
Data augmentation	Yes	No	No
Reweighting	Yes	No	No

trajectory and the previously computed object parabolic trajectory. Demonstrations with significant hand-object collisions are filtered out.

Throw. Throw demonstrations, which involve throwing objects with intentional velocity, are elegantly generated by time-reversing Catch trajectories. Interestingly, the parabolic motion of a thrown object is still physically reasonable due to the symmetrical nature of the parabola.

General Rotate. In addition to the simplified Rotate data generation method described in the main text, we also propose a more general approach for generating rotation data. This method produces more challenging data that requires longer training times. Specifically, we first select a grasp configuration g^1 from \mathcal{G} as the initial state and remove it from \mathcal{G} . We then iteratively find the closest grasp configuration in the remaining set: for each g^i , we search for its nearest grasp configuration g^{i+1} and remove g^{i+1} from \mathcal{G} ,



Fig. 10. Tracking a Regrasp Trajectory.

continuing this process for k steps. We transform all grasp configurations to align their wrist poses with that of g^1 . To provide sufficient buffer time to learn such large transitions, we replicate each g^i for N frames.

Regrasp. We define the Regrasp differs from Rotate in that it maintains a fixed object pose while transitioning between different hand configurations. The generation methodology mirrors that of Rotate, with the key distinction being that the grasp configurations are aligned to the same object pose rather than wrist pose.

Retargeting GRAB for Evaluation. We validated the system’s ability to track real-world HOI trajectories using sequences from the GRAB dataset [Taheri et al. 2020]. These were segmented into individual grasp–move–place episodes. An initial hand trajectory was obtained by retargeting based on the ManipTrans [Li et al. 2025] method, providing preliminary wrist and joint configurations. We further employed HOP to synthesize an improved grasp pose by fixing the object and wrist rotations from the initial grasp frame and optimizing the hand configuration toward higher grasp quality and physical plausibility while preserving kinematic similarity. The original finger and object data in each trajectory were replaced with this refined pose, yielding a corrected GRAB dataset that serves as a high-quality benchmark for evaluation.

11 Domain Randomization Settings

We employ domain randomization along three main axes: object scale, initial state, and a curriculum on observation/action noise.

Object scale randomization. During training, the object size is randomly perturbed to expose the policy to a range of geometries. At each environment reset, with probability 0.2 we uniformly sample a scale factor

$$s \sim \mathcal{U}(0.75, 1.5), \quad (13)$$

and uniformly scale the object by s . Otherwise, the object keeps its nominal size. This yields objects between 75% and 150% of the original scale across training episodes, resulting in improved generalization to geometric variations.

Random initial state. Beyond sampling a random reference frame from the motion dataset, we additionally inject controlled perturbations into the initial hand–object configuration to further enlarge the distribution of starting states. After selecting a trajectory and a time index, both the object pose and the hand configuration are perturbed using zero-mean bounded noise in a phase-dependent manner. For the object, let \mathbf{p}^o and R^o denote the sampled position and orientation. We add a stochastic positional offset

$$\mathbf{p}^o \leftarrow \mathbf{p}^o + \epsilon_p, \quad (14)$$

where the magnitude of ϵ_p is larger for non-contact frames—encouraging wider spatial variability—and smaller for contact frames to preserve

grasp stability. Rotational perturbations follow the same principle: non-contact frames receive full 3D angular noise up to a bounded angle, whereas contact frames use restricted in-plane perturbations to avoid breaking established grasps. For the hand, let \mathbf{q} and $\dot{\mathbf{q}}$ denote joint positions and velocities. Finger-joint angles are perturbed as

$$\mathbf{q} \leftarrow \mathbf{q} + \epsilon_q, \quad (15)$$

where ϵ_q is sampled within a bounded angular interval to encourage variability in finger postures, and joint velocities receive mild perturbations to model natural initialization variability. Tasks requiring substantial wrist reconfiguration further receive small perturbations on the wrist’s 6-DoF parameters, providing diverse but physically coherent wrist poses. All perturbations are applied stochastically and independently per environment, ensuring a broad yet physically valid distribution of initial states. Combined with random reference state sampling, this strategy significantly enhances robustness to variations in contact configuration, object placement, and hand posture at the start of each episode.

Curriculum on observation and action noise. We employ a two-stage curriculum to gradually increase the difficulty of the learning environment. During the first stage, training proceeds without object-scale variation, and the probability of applying random initial-state perturbations is kept relatively low. This allows the policy to establish stable behavior under moderately randomized but still well-structured conditions. In the second stage, object-scale randomization is activated, and the magnitude and frequency of initial-state perturbations are increased, exposing the policy to substantially richer geometric and dynamic variations. This staged progression introduces randomness in a controlled manner, enabling the policy to first acquire stable tracking behavior and then adapt to the full diversity of object scales and initial-state variability encountered during training.

12 LLM-based Trajectory Planning

We employ an LLM to generate semantically annotated keyframes and subsequently apply keyframe-guided interpolation in both position and orientation. This pipeline ensures the generated trajectories maintain both semantic coherence and dynamic feasibility, making them directly applicable to our tracking policy for practical manipulation tasks

LLM Prompt and Keypoint Specification. Given a high-level manipulation command (e.g., “upright a lying bottle”), we construct a structured prompt that includes: the task description, the initial wrist and object poses in a fixed robot base frame, the coordinate system definition, rotation conventions in XYZ Euler angles and quaternions, and smoothness constraints on positional and rotational changes. The prompt also provides a full desktop configuration listing all objects together with their feasible candidate grasp configurations, each associated with a valid wrist pose. The LLM is explicitly required to *select one* candidate grasp and align the generated grasp keypoint to that wrist pose.

The LLM outputs a JSON object containing keypoints and metadata. Each keypoint specifies a unique index, wrist position \mathbf{p}_i , orientation q_i , and an action label. Keypoints with *grasp* and *release* actions must be designated, with their indices explicitly provided in

Table 9. Multi-Task Distillation Performance Comparison

Method	Grasp								Move							
	Train				Test				Train				Test			
	SR [↑]	E_{op} [↓]	E_{or} [↓]	E_h [↓]	SR [↑]	E_{op} [↓]	E_{or} [↓]	E_h [↓]	SR [↑]	E_{op} [↓]	E_{or} [↓]	E_h [↓]	SR [↑]	E_{op} [↓]	E_{or} [↓]	E_h [↓]
Teacher	98.19%	1.03	6.20	3.74	73.89%	3.21	22.93	5.66	99.29%	2.31	10.57	4.12	99.14%	2.50	10.85	5.16
Student	97.88%	0.86	4.85	3.06	79.72%	2.50	20.76	4.81	98.25%	1.97	10.45	4.43	97.71%	2.27	10.68	3.95
Naive Multi-Task	66.01%	4.57	16.61	7.82	68.38%	5.32	17.39	7.59	81.40%	4.57	16.61	7.82	89.45%	3.17	11.76	5.56

Method	Place								Rotate							
	Train				Test				Train				Test			
	SR [↑]	E_{op} [↓]	E_{or} [↓]	E_h [↓]	SR [↑]	E_{op} [↓]	E_{or} [↓]	E_h [↓]	SR [↑]	E_{op} [↓]	E_{or} [↓]	E_h [↓]	SR [↑]	E_{op} [↓]	E_{or} [↓]	E_h [↓]
Teacher	98.41%	1.04	6.02	3.04	98.13%	1.09	8.42	2.85	97.30%	0.98	7.75	1.71	56.23%	2.38	44.96	2.57
Student	97.29%	1.15	7.39	3.03	97.32%	1.04	8.67	2.66	83.76%	1.49	11.23	2.28	45.44%	2.42	56.61	2.71
Naive Multi-Task	82.63%	3.49	29.02	5.77	84.88%	3.47	27.83	5.84	2.42%	2.27	27.67	4.75	0.39%	3.00	27.97	5.06

Table 10. Multi-Object Distillation Performance Comparison

Object	Pure Distill Policy (15 obj)				Distill&RL Policy (15 obj)				Distill&RL Policy (5 obj)				Sword Policy (1 obj)			
	Grasp	Move	Place	Avg	Grasp	Move	Place	Avg	Grasp	Move	Place	Avg	Grasp	Move	Place	Avg
Airplane	0.39	0.60	0.50	0.50	0.62	0.84	0.89	0.78	0.59	0.66	0.54	0.60	0.44	0.46	0.32	0.41
Ball	0.60	0.91	0.90	0.80	0.79	0.88	1.00	0.89	0.96	0.85	1.00	0.94	0.46	0.99	0.72	0.72
Basket	0.56	0.91	0.99	0.82	0.76	0.98	0.93	0.89	0.87	0.82	0.98	0.89	0.38	0.57	0.36	0.43
Book	0.14	0.59	0.41	0.38	0.51	0.83	0.74	0.70	0.33	0.53	0.61	0.49	0.15	0.45	0.30	0.30
Bottle	0.65	0.94	0.96	0.85	0.78	0.95	0.98	0.90	0.89	1.00	1.00	0.96	0.75	0.95	0.93	0.88
Bowl	0.38	0.78	0.74	0.63	0.76	0.79	0.80	0.78	0.62	0.76	0.62	0.67	0.22	0.56	0.11	0.30
Bowlround	0.64	0.88	0.84	0.78	0.86	0.89	0.85	0.87	0.84	0.91	0.85	0.86	0.38	0.43	0.08	0.30
Box	0.55	0.97	0.95	0.82	0.78	0.98	1.00	0.92	0.77	1.00	1.00	0.92	0.57	1.00	0.89	0.82
Eagle	0.28	0.67	0.42	0.46	0.45	0.51	0.73	0.56	0.46	0.67	0.52	0.55	0.28	0.53	0.27	0.36
Flower	0.22	0.62	0.53	0.46	0.44	0.65	0.66	0.59	0.35	0.56	0.49	0.46	0.26	0.58	0.38	0.41
Hammer	0.20	0.88	0.20	0.43	0.67	0.85	0.91	0.81	0.70	0.90	0.94	0.85	0.17	0.87	0.06	0.37
Hand	0.37	0.81	0.73	0.63	0.66	0.83	0.87	0.79	0.62	0.74	0.67	0.67	0.34	0.64	0.51	0.50
Headphones	0.53	0.93	0.89	0.78	0.71	0.97	0.94	0.87	0.68	0.87	0.84	0.80	0.64	0.86	0.75	0.75
Pencil	0.37	0.67	0.79	0.61	0.67	0.94	0.80	0.80	0.37	0.58	0.31	0.42	0.23	0.50	0.45	0.39
Pillow	0.11	0.52	0.44	0.35	0.30	0.61	0.67	0.53	0.14	0.45	0.43	0.34	0.09	0.42	0.50	0.34
Pizza	0.48	0.70	0.75	0.64	0.44	1.00	0.79	0.74	0.46	0.74	0.94	0.71	0.48	0.54	0.65	0.56
Spidermanfigure	0.31	0.69	0.45	0.48	0.59	0.53	0.71	0.61	0.40	0.70	0.46	0.52	0.29	0.61	0.30	0.40
Stapler	0.37	0.78	0.80	0.65	0.62	0.86	0.78	0.75	0.60	0.72	0.76	0.70	0.41	0.72	0.71	0.61
Sterilite	0.46	0.91	0.84	0.74	0.73	0.88	0.95	0.85	0.79	0.94	0.81	0.85	0.35	0.65	0.15	0.38
Sword	0.71	0.96	0.94	0.87	0.68	1.00	0.98	0.88	0.76	0.98	1.00	0.91	0.79	0.99	0.88	0.88
Wineglass	0.65	0.74	0.82	0.74	0.90	0.89	0.84	0.87	0.80	0.71	0.78	0.77	0.70	0.80	0.79	0.76
Average	0.43	0.78	0.71	0.64	0.65	0.89	0.85	0.80	0.62	0.77	0.74	0.71	0.40	0.67	0.48	0.52

top-level fields. These frames define interpolation segments, while start/end frames are derived from sequence boundaries. Other keypoints serve as internal anchors.

Keyframe-Based Piecewise Bezier Interpolation. The four special frame types naturally partition the LLM keypoints into three semantic segments: start \rightarrow grasp, grasp \rightarrow release, and release \rightarrow end. Within each segment, all keypoints (including intermediate approach/transport points) are used as interpolation anchors, while

Table 11. Hyperparameters

Parameter	Value	Parameter	Value	Parameter	Value
Σ_{π} Action Distribution Variance	0.055	λ^P Position	200 for Regrasp. 20 for Others	Initialization Disturbance Prob	0.5 for Regrasp. 0.3 for Others
Samples Per Update Iteration	65536	λ^r Rotation	200 for Regrasp. 20 for Others	Disturbance amplitude of dof	$\pi/8$
Policy/Value Function Minibatch Size	16384	λ^{op} Object Position	50	Disturbance amplitude of $dof vel$	0.1
γ Discount	0.99	λ^{or} Object Rotation	50	Disturbance amplitude of $obj vel$	0.02
Adam Stepsize	2×10^{-5}	$\lambda^{interact}$ Interaction	20	Disturbance amplitude of $obj rot$	0.02
GAE(λ)	0.95	$\lambda^{contact}$ Contact	5	λ^s Reweighting coefficient	10
TD(λ)	0.95	λ^{wp} Wrist Position	20		
PPO Clip Threshold	0.2	λ^{wr} Wrist Rotation	20		
Episode Length	60				

different segments are interpolated independently. For each segment, we construct a cubic Bezier curve for the wrist position using the segment endpoints as Bezier endpoints and generating two inner control points from finite differences of neighboring anchors, so that the curve tangents align with the discrete motion directions proposed by the LLM. We then sample a fixed number of trajectory points per LLM keypoint and concatenate all segments into a dense position trajectory, removing duplicated boundary samples. This piecewise scheme ensures smooth motion inside each phase while strictly preserving the grasp and release boundaries (e.g., if the LLM predicts indices 3 and 8 as grasp and release, we only interpolate within [1,3], [3,8], and [8,9]).

Orientation Interpolation. Wrist orientations are interpolated independently of positions. We first convert all keyframe orientations to quaternions, enforce sign continuity along the sequence to avoid double-cover flipping, and then apply spherical linear interpolation (SLERP) within each segment using the same temporal parameterization as for the position Bezier curves. Segments with negligible rotation are treated as “static” and the orientation

The trajectories generated by both the LLM and Text2HOI [Cha et al. 2024] are subsequently processed by HOP, which replaces the original finger degrees of freedom with synthesized grasp poses.

13 Policy Distillation

To address skill interference in multi-task and multi-object learning, we implement a progressive knowledge distillation framework that systematically transfers expertise from specialized teacher policies to a unified student policy. Inspired by previous work [Luo et al. 2023; Xu et al. 2025], we employ a four-stage training strategy: **Stage I** (0-500 epochs) utilizes pure DAgger algorithm for behavioral cloning, where student actions are entirely sampled from teacher policies and updated using expert supervision loss (ELoss). **Stage II** (500-5000 epochs) introduces hybrid decision-making through expert mode masking, with teacher action sampling probability linearly decaying from 100% to 0% to enable smooth autonomy transition. **Stage III** (5000-7000 epochs) focuses on value function optimization, progressively incorporating policy gradient loss when explained variance (EV) consistently exceeds 0.6 for three consecutive evaluation windows. **Stage IV** (7000+ epochs) employs comprehensive

loss balancing combining policy gradient, value function, boundary constraints, and residual expert supervision losses, dynamically weighted based on training progress and critic performance.

To evaluate the effectiveness of policy distillation, we compare the performance of teacher policies, the distilled student policy, and a naively trained multi-task policy on a composite tracking task involving four meta-skills: Grasp, Move, Place, and Rotate. As shown in Tab. 9, the distilled student policy significantly mitigates skill interference commonly observed in multi-task learning, yielding a 28.5% improvement on the challenging Rotate skill. Moreover, the distillation process reduces the required training cycles by approximately 45% while achieving higher final performance compared to naive multi-task training.

To evaluate how distillation improves generalization across objects, we conduct experiments on the Grasp, Move, and Place skill data under several training settings: a student policy distilled (without RL) from 15 objects; a student policy using both distillation and RL with 15 objects; a Distill&RL policy trained on 5 objects; and a policy trained on a single object (Sword). As shown in Tab. 10, the Distill&RL approach yields clear gains over pure Distill alone. Moreover, performance improves consistently as the number of training objects increases, confirming the benefit of multi-object training for generalization.

14 Limitations and Discussions

While our method presents a promising path to addressing the data bottleneck in dexterous manipulation, several limitations remain. First, although HOP provides a general-purpose low-level control capability for trajectory tracking, and we have demonstrated its integration with high-level planners such as LLMs [Achiam et al. 2023] and Text2HOI [Cha et al. 2024], the current high-level planners operate in an open-loop manner. They do not yet support long-horizon, closed-loop task execution like an LLM-based agent. For example, when an object is dropped, the system lacks the capability to autonomously regenerate a recovery trajectory. Achieving such robustness requires advances in both more adaptive tracking policies and more reactive, long-horizon planners.

Second, although we have defined and evaluated seven meta-skills, learning a unified policy that generalizes across all seven skills and a large set of objects remains challenging. Skills such as Regrasp, while tractable for individual objects (See Fig. 10), become

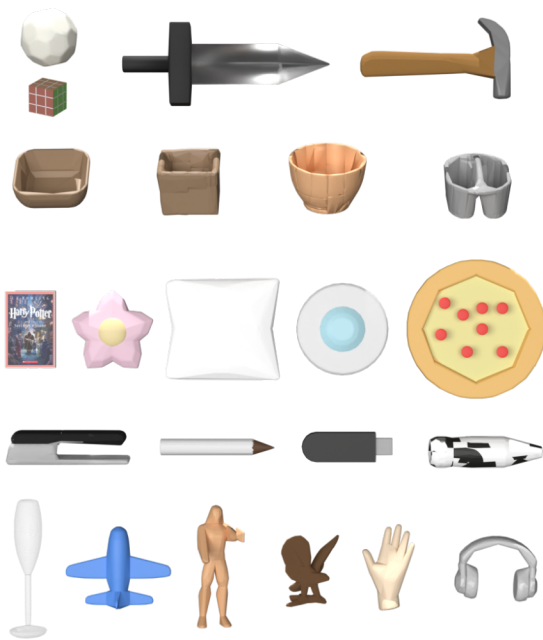


Fig. 11. Objects Used For Training and Testing.

increasingly difficult to learn as object diversity grows. Scaling to more complex skills and broader object categories may require large-scale, learning-based refinement of HOP data and hierarchical distillation strategies.

Furthermore, real-world deployment faces the sim-to-real gap, particularly for the highly dynamic motions that our method excels at in simulation. This demands hardware with high control frequency and force-sensing capabilities—features that remain limited in current robotic hands.

Overall, this work demonstrates the feasibility of a general-purpose dexterous controller learned from synthetic data, yet several open challenges remain for further scaling and real-world application.

15 Hyperparameters

We have compiled all simulation parameters, training hyperparameters, reward function coefficients, and data augmentation settings in Tab. 11.